A cohesin-independent mechanism modulates recombination activity along meiotic chromosomes

Jonna Heldrich[1], Tovah E. Markowitz[1,#], Luis A. Vale-Silva[1], and Andreas Hochwagen[1,*]

[1] Department of Biology, New York University; New York, NY 10003; USA

[#] Current address: Leidos Biomedical Research, Inc.; Bethesda, MD; USA

[*] Correspondence: andi@nyu.edu

Running title: Cohesin-independent recruitment of meiotic axis proteins

Summary

Meiotic chromosomes organize around a cohesin-dependent axial element, which promotes meiotic recombination and fertility. In the absence of cohesin, axial-element proteins instead accumulate in poorly understood genomic regions. Here, we show in *S. cerevisiae* that these regions are particularly enriched for axis proteins even on wild-type chromosomes and thus reflect a cohesin-independent recruitment mechanism. By contrast, other organizers of chromosome structure, including cohesin, condensin, and topoisomerases, are depleted from the same regions. This spatial patterning is observable before meiotic entry and therefore independent of meiotic recombination. Indeed, the regional density of gene-coding sequences is sufficient to predict a large fraction of cohesin-independent axis protein binding, suggesting that the gene-associated chromatin landscape plays a role in modulating axis protein deposition. The increased accumulation of axis proteins in these regions corresponds to a greater potential for initiation of recombination and progression to crossovers.

Key words: Synaptonemal complex, Rec8, Red1, Hop1, DSB hotspot, nucleosomes, Rtf1

Introduction

Inheritance of genetic information in sexually reproducing organisms depends on a reductional cell division called meiosis [1–3]. This process involves the dangerous yet necessary infliction of DNA double-strand breaks (DSBs), which lead to exchange of DNA between homologous chromosomes during meiotic recombination. Meiotic DSBs occur within the framework of a complex 3D organization of the genome, which promotes compaction, individualization, pairing and repair of chromosomes in preparation for chromosome segregation during the first of the two meiotic divisions. Chromosomes fold into loops that are anchored together at their bases by the axial element, a proteinaceous scaffold made up of meiosis-specific axis proteins that, in the budding yeast *Saccharomyces cerevisiae*, include Red1, Hop1, and Rec8-cohesin [4,5]. The axial element provides binding sites for accessory factors essential for DSB formation and is required for both normal levels and normal distribution of meiotic DSBs [6–8].

The placement of axial-element proteins is largely determined by cohesin, which localizes axis proteins to discrete sites along the chromosomes and finetunes their binding to gene ends [6,7]. In the absence of Rec8, no axis structure is detectable by electron microscopy and loop formation is disrupted [9,10]. In yeast and plant r*ec8* mutants, axis proteins nevertheless continue to bind chromosomes, albeit at reduced levels and in an aberrant pattern [6,7,11,12] (**Figure 1A-C**). In these mutants, DSB formation is generally restricted to regions that retain axis protein binding [6,7,12]. Here, we show that this retention of axis proteins reflects a Rec8-independent recruitment mechanism for axis proteins that is also active during wild-type meiosis. We show that this patterning is independent of meiotic entry, that regional gene density is sufficient to predict a substantial fraction of axis-protein distribution, and that the regional enrichment of axis proteins is associated with greater levels of DSB and crossover activity on wild-type chromosomes.

Results

Definition of regions of axis-protein enrichment

To define the regions associated with axis-protein enrichment bioinformatically, we reanalyzed ChIP-seq data of the yeast axis component Red1 in a *rec8*Δ mutant by dividing the genome into windows and setting an enrichment threshold (see **Methods**). Windows with Red1 signal above the threshold were joined with immediately adjacent windows of significant Red1 signal, and these genomic regions were termed clusters (**Figure 1C**). The intervening regions were defined as deserts.

As shown previously [6,7], clusters are distributed in a nonuniform pattern across the 16 yeast chromosomes (**Figure 1C**). The size, number, and relative positions of clusters vary for each chromosome and show no obvious association with centromeres or telomeres. One consistent pattern that distinguishes the small chromosomes (I, III, VI) is their almost complete coverage by clusters, while the large chromosomes are overwhelmingly made up of deserts.

Differential enrichment of core axis factors along wild-type chromosomes

We wondered whether the biased binding of Red1 in clusters also occurs on wild-type chromosomes. We analyzed existing ChIP-seq data of axis factors obtained from wild-type yeast at 3 hours after meiotic induction [7,13], the time when meiotic DNA breakage is maximal [14]. This analysis showed that even in wild-type cells, Red1 binds significantly more in cluster regions than in deserts (**Figure 1B, D** and **Figure S1A**).

One reason for this differential enrichment could be the fact that axis attachment sites, defined as peaks of enrichment of the axis proteins Red1, Hop1, and Rec8, are more densely spaced in clusters (**Figure 1E**). However, axis-protein binding levels at these sites do not support this hypothesis. Whereas Red1 and Hop1 were indeed significantly more enriched at axis sites

located in cluster regions (**Figure 1H-I**), Rec8 was more enriched at axis sites in deserts (**Figure 1J**). Another component of the cohesin complex, Scc2, bound with the same trends as Rec8 (**Figure 1K**). The complementary enrichment of Red1/Hop1 and cohesin implies the existence of a second recruitment mechanism that recruits Red1 and Hop1 to wild-type chromosomes without cohesin.

In line with this interpretation, the extra enrichment of Red1 and Hop1 in clusters is not spatially connected to cohesin-dependent enrichment peaks. This additive effect was particularly obvious when analyzing Red1 enrichment across gene bodies. Metagene analysis showed a uniform increase of Red1 binding in the cluster regions overlaid over the biased recruitment to gene ends mediated by Rec8 (**Figure 1F-G**). These data indicate that the second recruitment mechanism creates broad domains of enrichment and acts in parallel to the focal axis-protein enrichment mediated by Rec8-cohesin.

In the absence of Rec8, chromosomal association of Red1 becomes fully dependent on Hop1 [7], raising the possibility that Hop1 helps mediate cohesin-independent recruitment of Red1 on wild-type chromosomes. Indeed, analysis of Red1 enrichment in a *hop1*Δ mutant showed Red1 enriched in deserts rather than clusters (**Figure 1L**), matching the pattern of Rec8 (**Figure 1J**). This outcome is in keeping with the notion that Red1 binding becomes fully dependent on cohesin in the absence of Hop1 [7]. We conclude that Hop1 is responsible for cohesin-independent recruitment of Red1.

Differential enrichment in clusters and deserts does not require meiotic entry

Further analysis showed that three additional regulators of meiotic chromosome structure, condensin, topoisomerase I (Top1) and topoisomerase II (Top2), are also differentially distributed between these regions on wild-type chromosomes. Analysis of available ChIP-seq

data of PK9-tagged Smc4, a subunit of condensin [13], Top1-13myc, and Top2 [15] showed significantly greater binding of all three proteins around axis sites in deserts compared to clusters (**Figure 1M-O**). Desert enrichment of Top1 and Top2 was even more apparent at DSB hotspots (**Figure S1B-C**), which often overlap with peaks of topoisomerase enrichment [15]. Notably, the biased enrichment of Top2 in deserts was also observed in the absence of meiotic DSBs (*spo11-YF* and *spo11*Δ) (**Figure S1D-E**). Indeed, topoisomerases and condensin were enriched in deserts even in premeiotic or cycling cells (**Figure S1F-H**). These data indicate that the signals differentiating clusters and deserts are not linked to the meiotic program.

Mutant analysis did not reveal obvious roles for condensin or Top2 in defining clusters and deserts. Conditional nuclear depletion of the condensin subunit Brn1 by anchor-away [16] caused vegetative cell lethality [17] but did not alter the relative enrichment of Red1 in cluster regions (**Figure S1I-J**). Similarly, inactivation of *TOP2*, using the temperature-sensitive *top2-1* allele at 34°C [15,18], had no effect on the greater relative enrichment of Red1 and Hop1 in clusters (**Figure S1K-N**). Although we cannot exclude redundant effects, our data indicate that neither cohesin, nor condensin or Top2 alone are responsible for differentiating cluster and desert regions.

Clusters are associated with longer genes and increased coding density

The apparent independence from the meiotic program prompted us to investigate whether inherent chromosomal features could explain the formation of clusters and deserts. Previous analysis of Red1 enrichment in *rec8* mutants had indicated that long genes are significantly over-enriched in regions of Red1 binding [7]. Consistent with this analysis, we found that the median length of open reading frames in clusters was 17.6% greater than in deserts (clusters = 1433 bp; deserts = 1218 bp) (**Figure 2A**). By contrast, deserts exhibited significantly larger intergenic regions (**Figure 2B**). The greatest difference was observed for divergent regions,

which had an 85.6% (~279 bp) larger median size in deserts than in clusters, but the same trend was also observed for tandem regions (39.4% or ~124 bp larger in deserts) and convergent regions (29.4% or ~55bp larger in deserts). These data indicate that clusters are associated with both increased gene size and increased coding density.

The median sizes of clusters and deserts are approximately 15 kb and 22.5 kb, which correspond to around 9 and 14 genes, respectively, and raises the possibility that cluster formation may be a regional effect. Indeed, logistic fit analysis after segmenting the genome into 5-kb bins showed a strong bias toward high coding density (coding nucleotides/total DNA) in bins defined as clusters (**Figure 2C**).

To probe the significance of this regional association in explaining axis protein recruitment, we trained a logistic regression model, using 80% of the genome as a learning set for predicting clusters and deserts in the remaining 20% based on coding density. This approach showed that nearly 70% of the test set could be accurately predicted as either a cluster or a desert based on the regional coding density alone (coding nucleotides/total DNA per 5kb window) (**Figure 2D**). This number improved only marginally to 72.5% when we excluded the short chromosomes (**Figure S2A-B**), indicating that known cis-encoded features that increase recombination activity on short chromosomes [19–21] have only minor impact on the overall performance of this model. Thus, regional coding density is a major predictor of axis-protein cluster formation.

We also observed a substantial effect of cluster size on Red1 enrichment. When clusters were separated into 3 quantiles by length, average Red1 enrichment per bp scaled significantly with cluster length (based on 95% C.I.; **Figure 2E**). This association implies that larger cluster regions are better able to recruit or retain Red1 binding.

Nucleosome occupancy and order is elevated in clusters

We speculated that the higher coding density of clusters could be manifested in a different overall chromatin state, as genes in the *S. cerevisiae* genome are typically associated with well-ordered nucleosomes [22]. Therefore, we used published data to analyze nucleosome enrichment patterns in clusters and deserts. Analysis of the ChIP-seq signal of histones H3 [23] and H4 [24] during meiotic prophase showed a significant enrichment of both histones in cluster regions (**Figure 3A-B**). Similar results were observed after micrococcal nuclease digestion (MNase-seq) of meiotic prophase samples [15,25] (**Figure 3C-D**), as well as prior to meiotic entry (0h; **Figure S3A**). Clusters also exhibited a more pronounced signal periodicity (**Figure 3C**), indicating that nucleosomes are more highly ordered than in deserts. This higher spatial order is also apparent when specifically analyzing MNase-seq patterns around meiotic DSB hotspots (**Figure 3D**).

We investigated whether differences in nucleosome stability or periodicity could underlie the formation of clusters and deserts. The acetylation of histone H4 on lysine 44 (H4K44ac) regulates nucleosome stability in meiosis and has been implicated in meiotic DSB activity [24]. Analysis of existing ChIP-seq data showed an enrichment of H4K44ac around hotspots located in clusters (**Figure 3E**), but this enrichment was largely explained by the higher nucleosome levels in these regions (**Figure 3F**) and is also seen for H3K4me3, another hotspot-associated histone modification (**Figure 3G-H**). However, MNase-seq data showed that the differential enrichment of nucleosomes around hotspots in cluster regions persisted in a non-acetylatable H4K44R mutant (**Figure S3B-C**). Thus, H4K44ac-associated nucleosome turnover cannot explain the different levels of nucleosomes in clusters versus deserts.

To probe the role of nucleosome order in establishing clusters and deserts, we analyzed mutants lacking the PAF1C subunit Rtf1, which has been implicated in nucleosome positioning

[26]. MNase-seq analysis of *rtf1*Δ mutants revealed reduced nucleosome order along genes, as indicated by the less pronounced periodicity of nucleosome peaks in clusters relative to the +1 nucleosome (**Figure S3D-E**). However, the relative enrichment of Red1 in clusters was unaffected by the absence of *RTF1* (**Figure S3F**), indicating that Red1 binding in clusters is not affected by altered nucleosome order. Accordingly, Red1 enrichment in clusters was also unaffected by the loss of Set1 and Dot1, two histone methyltransferases that are regulated by PAF1C in meiosis and promote Red1 binding [11,27] (**Figure S3G-H**). Together, these analyses exclude several known modulators of meiotic chromatin states as regulators of cluster and desert formation.

Meiotic recombination activity is more frequent in clusters

As Red1 and Hop1 are necessary to support wild-type levels of meiotic DSB formation and recombination, we asked whether the differential enrichment of axis proteins had functional consequences for meiotic recombination along wild-type chromosomes. As expected from the narrower nucleosome-free regions in clusters (**Figure 3D**), average Spo11-oligo levels, which report on meiotic DSB distribution [25,28] showed a more focused peak for hotspots located in clusters compared to desert hotspots (**Figure 4A-C**). In addition, average Spo11 activity per bp was elevated in cluster hotspots (**Figure 4C)**, suggesting more concentrated DSB formation. Indeed, the area under the Spo11-oligo curve was mildly but significantly greater at cluster hotspots (**Figure S4A**), even though the density of hotspots did not differ between clusters and deserts (**Figure S4B**), indicating that hotspots in cluster regions have on average a higher likelihood of initiating meiotic recombination. Consistent with higher DSB activity, sequences surrounding cluster hotspots also saw a greater enrichment of histone H2A phosphorylated on serine 129 (pH2A), an indicator of meiotic DSB activity (**Figure 4D-E**), although this enrichment is partly driven by the greater histone occupancy in clusters (**Figure S4C**).

We asked whether the higher enrichment of axis proteins in clusters also impacts the chance of crossover repair in these regions. The SUMO ligase Zip3 governs the designation of DSBs for crossover repair and is a cytological and genomic marker of crossover designation [29–31]. Indeed, analysis of published Zip3 ChIP-seq data [31] indicated a greater enrichment of Zip3 at cluster hotspots (**Figure 4F-G**). These data imply that cohesin-independent enrichment of axis proteins leads to regions of increased recombination activity on wild-type chromosomes.

Discussion

Here, we show that the previously observed regional enrichment of axis proteins in yeast *rec8* mutants [6,7] reflects a second, cohesin-independent mechanism for axis-protein recruitment that is active in wild-type cells and impacts the frequency of meiotic recombination activity along meiotic chromosomes. Similar cohesin-independent association of axis proteins is also observed in *Arabidopsis thaliana* [12], suggesting that this mechanism may be conserved.

Cytological experiments in yeast have revealed chromosomal domains of differential axis protein enrichment that also have a higher chance of exhibiting Zip3 foci [32–34]. Therefore, it is tempting to speculate that the cluster and deserts defined here reflect the domains defined by cytology. The uniform enrichment of axis proteins in cluster regions, although mild overall, could indeed be broad enough to be cytologically observable. Moreover, axis protein-rich domains alternate with regions enriched for Rec8-cohesin by cytology [34], in line with our analyses. One argument against a direct correspondence is that enrichment of Hop1 in clusters is unchanged in mutants lacking the chromosome remodeler Pch2 (**Figure S1O**), whereas the cytological domains disappear in *pch2* mutants (Börner et al., 2008), but this could be an effect of higher Hop1 signal masking the underlying structure.

The differential enrichment between clusters and deserts is also seen for several other chromosome structure factors, including condensin and topoisomerases, implying that these regions exhibit fundamental differences in chromosome or chromatin organization. Cohesin, condensin, and topoisomerases are all enzymes that can alter chromosome structure [35–38], suggesting that deserts are structurally more active than cluster regions. However, our analyses found no evidence that this structural activity displaces axis proteins from deserts. Alternatively, structural activity could come from processes such as transcription, because genes in clusters have on average lower steady-state mRNA levels (16.1% smaller median) than genes in deserts during early prophase (**Figure S4D**). Arguing against this possibility is the fact that the transcriptional program changes dramatically as cells enter the meiotic program [15,39,40], yet clusters and deserts can be detected even prior to meiotic entry by the differential enrichment of nucleosomes, topoisomerases, and condensin. We therefore favor the interpretation that the differential distribution of chromosome structure factors is a secondary consequence of inherent properties of the chromatin fiber.

The notion that the features differentiating clusters and deserts are to a large extent hard-wired into the local chromatin environment is supported by our finding that regional coding density can predict approximately 70% of the cluster and desert regions. The fact that the elevated axis protein enrichment in clusters occurs uniformly across gene bodies suggests that the feature recruiting axis proteins may be relatively broad and non-specific. One such feature that clearly differentiates clusters is the higher density and order of nucleosomes. However, altering nucleosome order did not affect Red1 binding in clusters, arguing against a role for this feature in recruiting axis proteins. We also excluded roles for two histone methyltransferases, Set1 and Dot1, which are required for wild-type levels of Red1 recruitment [11]. It is possible that other chromatin marks or even inherent nucleosomal features, such as unmodified histone surfaces or the associated DNA conformations, could create a broad signal that modulates binding of

axis proteins, but this question requires further investigation. Intriguingly, the axis factor Hop1, which is required for Red1 recruitment to cluster regions ([7] and this study), binds structured DNA in vitro [41,42]. Thus, a better understanding of Hop1 in vivo chromatin binding activities may help identify the chromatin features differentiating clusters from deserts.

Ultimately, the cohesin-independent enrichment of axis proteins has consequences for meiotic recombination. Clusters exhibit elevated levels of meiotic DSB formation and DNA damage signaling, and indeed are the only sequences that show substantial levels of meiotic DSB formation in *rec8* mutants [6–8]. Importantly, clusters also exhibit significantly higher levels of the crossover marker Zip3, which is essential for regularly spaced crossover formation [30,31,43]. Thus, our data identify a novel layer of crossover regulation that modulates the patterns of recombination along meiotic chromosomes.

Acknowledgements

We thank N. Hollingsworth for sharing antibodies, G. Vader for helpful discussions, and the NYU Department of Biology Sequencing Core for technical assistance and data processing. This work was supported by the National Institutes of Health [GM111715 and GM123035 to AH].

Author contributions

Conceptualization, J.H., T.E.M. and A.H.; Investigation, J.H., T.E.M., L.A.V.S., and A.H.; Software, J.H.; Formal analysis, J.H., T.E.M. and A.H.; Resources, J.H., T.E.M. and A.H.; Writing – Original Draft, J.H and A.H.; Writing – Review & Editing, J.H., T.E.M., L.A.V.S., and A.H.

Declaration of Interests

The authors declare no competing interests.

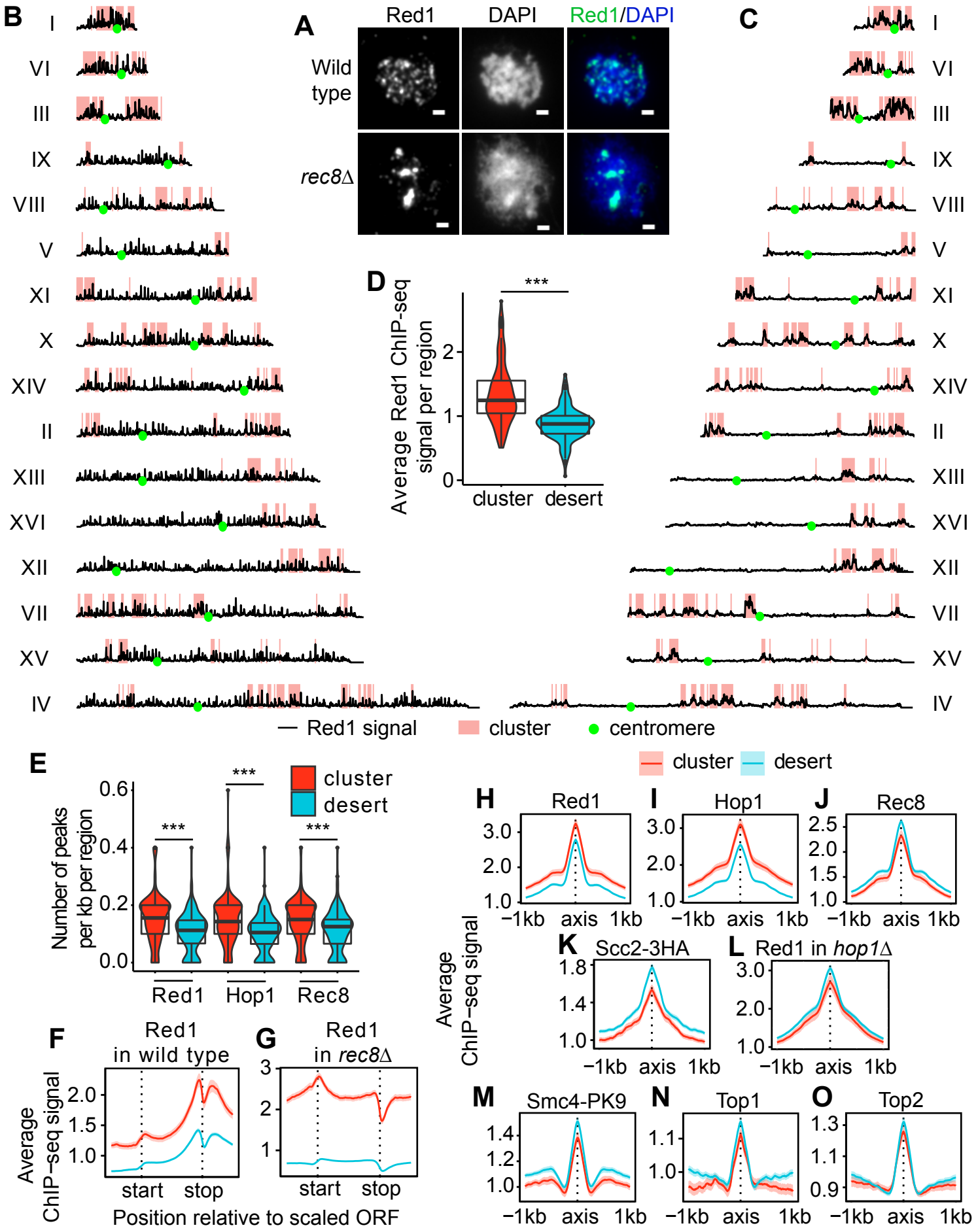
B
A
Red1
DAPI
Red1/DAPI
Wild type
rec8Δ
C
D
Average Red1 ChIP-seq signal per region
***
cluster
desert
Red1 signal
cluster
centromere
E
Number of peaks per kb per region
Red1
Hop1
Rec8
F
Red1 in wild type
G
Red1 in rec8Δ
Average ChIP−seq signal
start
stop
Position relative to scaled ORF
H
Red1
I
Hop1
J
Rec8
K
Scc2-3HA
L
Red1 in hop1Δ
M
Smc4-PK9
N
Top1
O
Top2
−1kb
axis
1kb

Figure 1

Figure Legends

Figure 1. Cohesin-independent recruitment of axial elements boosts Red1 binding in wild type.

(A) Representative images of immunofluorescence staining for Red1 (green) and DAPI (blue) on chromosome spreads of wild-type and *rec8*Δ mutant cells 5 hours after meiotic induction. Bar, 1 μm. (B) Wild-type and (C) *rec8*Δ genomic distribution of Red1 (black) on all chromosomes at the time of DSB formation (3 hours after meiotic induction) as measured by ChIP-seq. Red underlay delineates regions designated as clusters. Green dots mark the centromeres. (D) Violin and box plots quantifying the average Red1 signal per cluster or desert region on wild-type chromosomes. ***$P < 0.0001$, *t*-test. (E) Quantification of the density of Red1, Hop1, and Rec8 peaks per kb of cluster (red) and desert (blue) regions. ***$P < 0.0001$, Mann-Whitney-Wilcoxon test. Metagene analysis of Red1 in wild type (F) and *rec8*Δ (G) indicating average ChIP-seq enrichment along genes in clusters and deserts. Average Red1 (H), Hop1 (I), Rec8 (J), Scc2-3HA (K), Red1 in *hop1Δ* (L), Smc4-PK9 (M), Top1 (N), and Top2 (O) binding in wild type at axis attachment sites [13] in clusters and deserts. The 95% confidence interval for the average lines is shown for **H-O**. See also Figure S1.

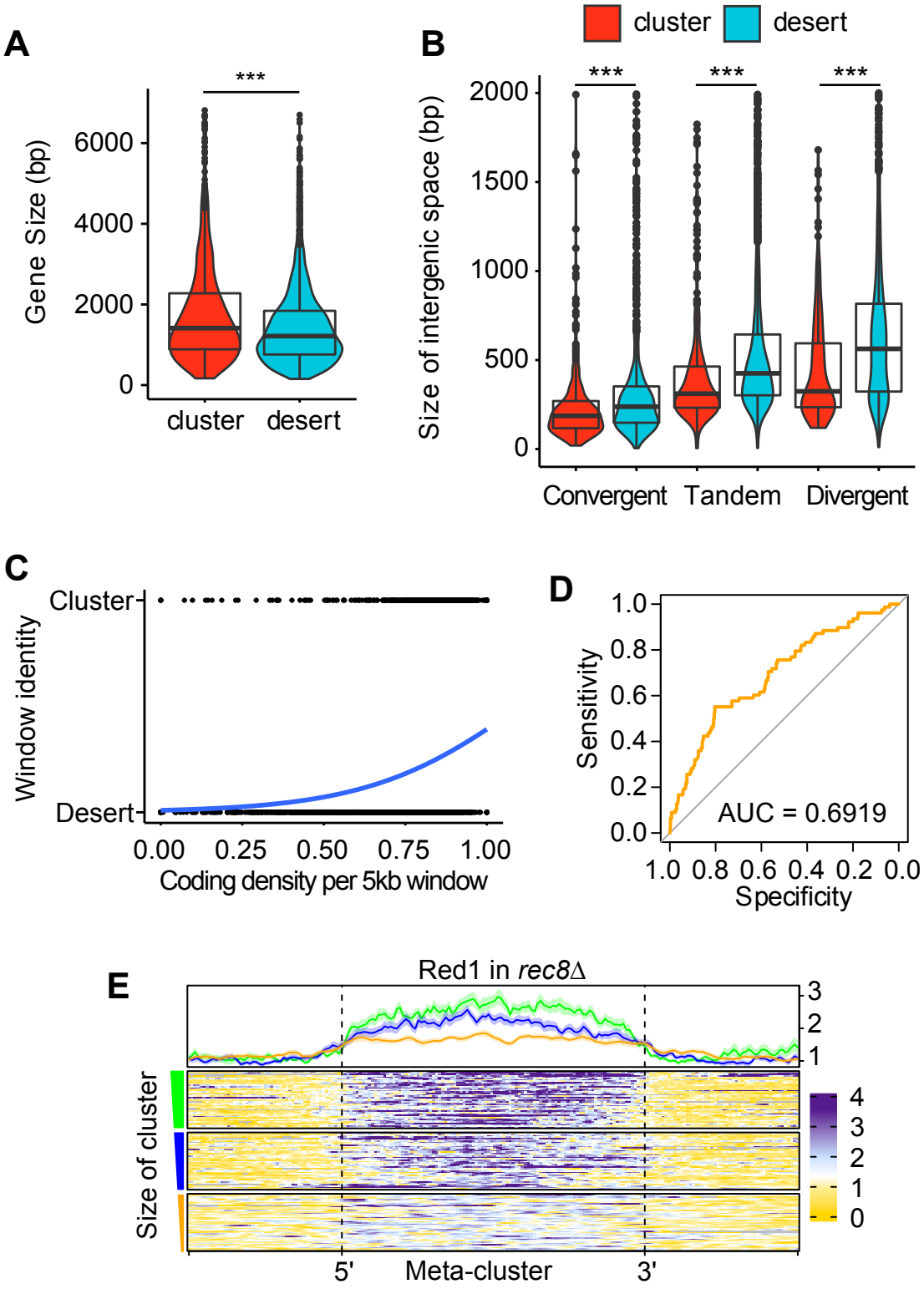
A
Gene Size (bp)
6000
4000
2000
0
***
cluster
desert
B
cluster
desert
Size of intergenic space (bp)
2000
1500
1000
500
0
***
***
***
Convergent
Tandem
Divergent
C
Window identity
Cluster
Desert
0.00
0.25
0.50
0.75
1.00
Coding density per 5kb window
D
Sensitivity
1.0
0.8
0.6
0.4
0.2
0.0
AUC = 0.6919
1.0 0.8 0.6 0.4 0.2 0.0
Specificity
E
Red1 in rec8Δ
3
2
1
Size of cluster
4
3
2
1
0
5'
Meta-cluster
3'

Figure 2

Figure 2. Clusters are composed of long, closely spaced genes.

(A) The distribution of the gene sizes in clusters (red) and deserts (blue) displayed in violin and box plots. (B) The distribution of the sizes of convergent, tandem, and divergent regions in clusters (red) and deserts (blue). For (A-B), ***$P < 0.0001$, Mann-Whitney-Wilcoxon test. (C) Distribution of the coding density in 5-kb cluster windows and their identity assignment as clusters or deserts. The blue line indicates the fitted curve for the data. The coding density was chosen as a significant feature in training a logistic regression model ($P < 0.0001$). (D) ROC curve showing the specificity versus sensitivity of prediction of a subset of 20% of test data. The area under the curve (AUC) is 0.6919. (E) Meta analysis of Red1 ChIP-seq signal in *rec8*Δ in cluster regions sorted by size of the region (small = below 10 kb; medium = 10 kb to 40 kb; large = 40 kb to 210 kb). Averages for each quantile are shown above the heatmap, and the 95% confidence interval for the average lines is shown. See also Figure S2.

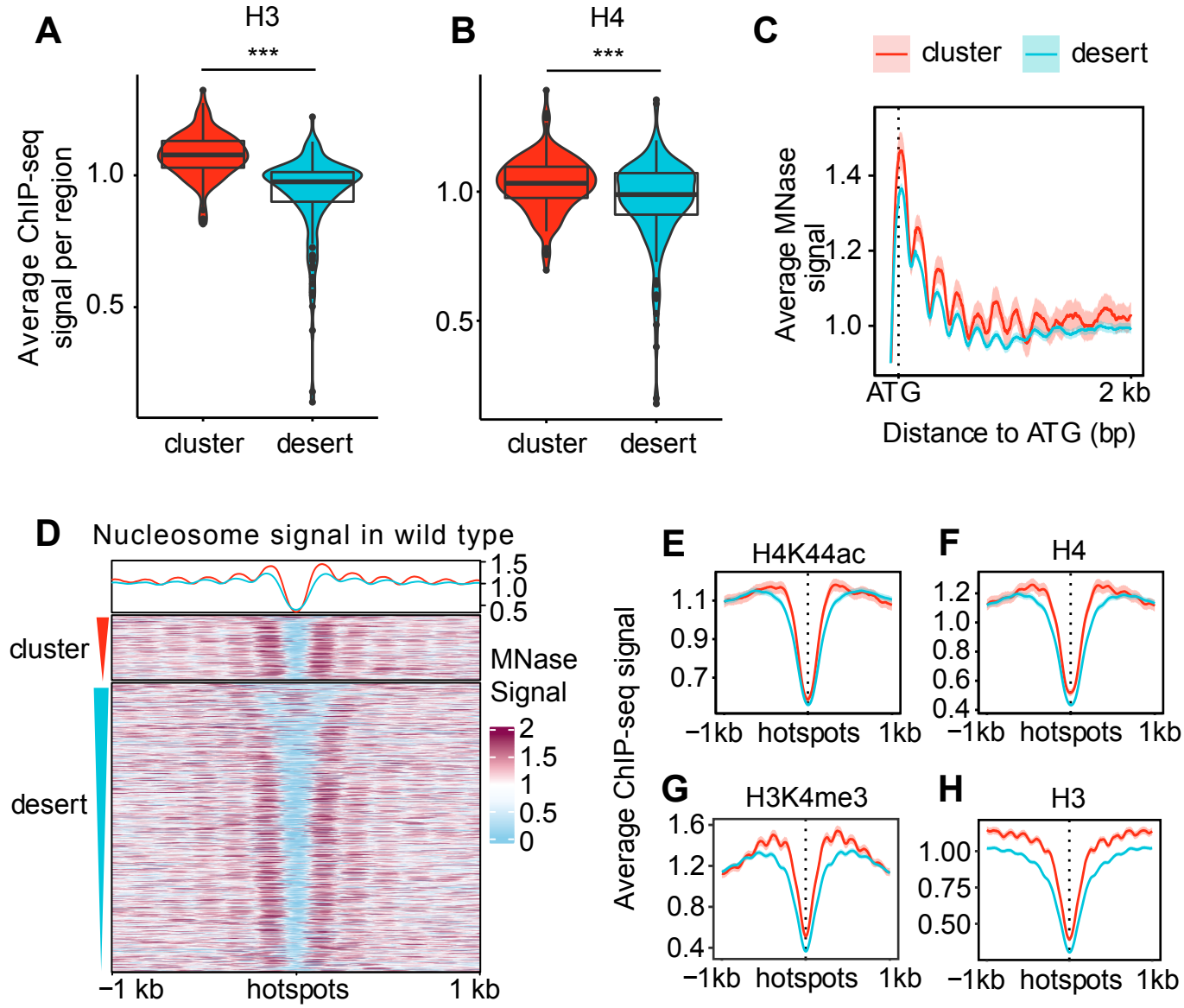
A
H3
***
Average ChIP-seq signal per region
1.0
0.5
cluster
desert
B
H4
***
1.0
0.5
cluster
desert
C
cluster
desert
Average MNase signal
1.4
1.2
1.0
ATG
2 kb
Distance to ATG (bp)
D
Nucleosome signal in wild type
1.5
1.0
0.5
cluster
desert
MNase Signal
2
1.5
1
0.5
0
−1 kb
hotspots
1 kb
E
H4K44ac
F
H4
Average ChIP-seq signal
1.1
0.9
0.7
1.2
1.0
0.8
0.6
0.4
−1kb
hotspots
1kb
G
H3K4me3
H
H3
1.6
1.2
0.8
0.4
1.00
0.75
0.50

Figure 3

Figure 3. **Hotspots in clusters are located in narrow intergenic regions surrounded by highly ordered nucleosomes.**

Violin and box plots quantifying the average (A) H3 [23] and (B) H4 [24] signal per cluster or desert region on wild-type chromosomes at 4h after meiotic induction. ***$P < 0.0001$, Mann-Whitney-Wilcoxon. (C) Average MNase signal for clusters (red) and deserts (blue) lined up at the ATG for every gene. (D) Heatmap of wild-type MNase signal centered at all hotspot midpoints [28], separated into cluster or desert regions and sorted by width of hotspots. The average signal in clusters and deserts is plotted above the heatmap. Average H4K44ac (E), H4 (F), H3K4me3 (G), and H3 (H) ChIP-seq signal lined up at hotspots in clusters and deserts. The 95% confidence interval for the average lines is shown for all averaged signals. See also Figure S3.

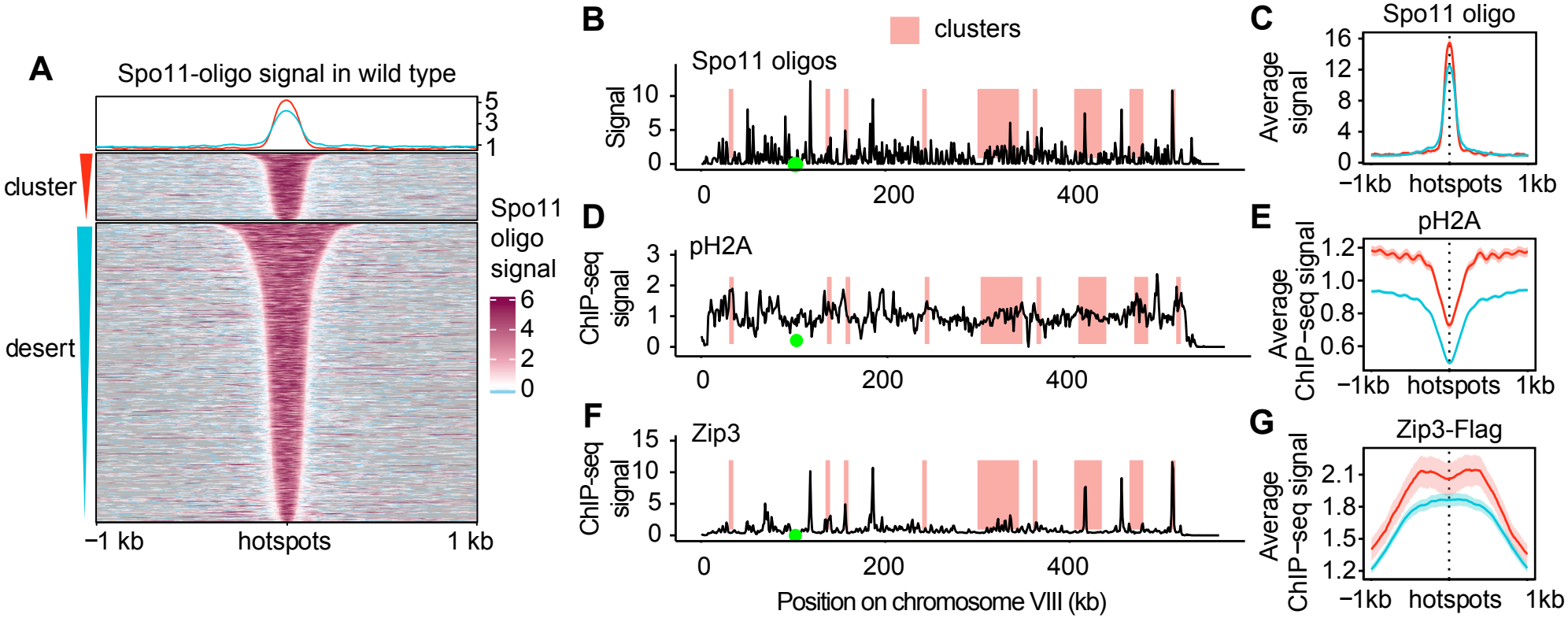
A
Spo11-oligo signal in wild type
cluster
desert
Spo11 oligo signal
−1 kb
hotspots
1 kb
B
clusters
Spo11 oligos
Signal
Position on chromosome VIII (kb)
C
Spo11 oligo
Average signal
−1kb
hotspots
1kb
D
pH2A
ChIP-seq signal
E
pH2A
Average ChIP−seq signal
F
Zip3
G
Zip3-Flag

Figure 4

Figure 4. DNA breakage and crossover designation are more frequent in clusters.

(A) Heatmap of Spo11-oligo signal [28] at 4h after meiotic induction centered at all hotspot midpoints, separated into cluster or desert regions, and sorted by size of hotspots. The average of signal in clusters (red) and deserts (blue) is plotted above the heatmap. Spo11-oligo signal (B-C) and ChIP-seq analysis of pH2A at 3h after meiotic induction (D-E) and Zip3 at 4h after meiotic induction [31] (F-G). The pH2A dataset was from an *ndt80*Δ mutant, which is unable to exit meiotic prophase but shows no obvious defects at 3h after meiotic induction [44]. (B, D, F) Signal on wild-type chromosome *VIII*. Red underlay represents clusters, and green dot marks centromere. (C, E, G) Average signal on wild-type chromosomes at cluster and desert hotspots. The 95% confidence interval for the average lines is shown. See also Figure S4.

Materials and Methods

Yeast strains and growth conditions

All strains used in this study were of the SK1 background, with the exception of the *top2-1* mutant, which is congenic to SK1 (backcrossed >7x). The genotypes are listed in **Table S1**. To induce synchronous meiosis, strains were accumulated in G1 by inoculating BYTA medium with cells at OD600 = 0.3 for 16.5 hours at 30°C [14]. Cultures were washed twice with water and resuspended into SPO medium at OD600 = 1.9−2.0 at 30°C as described [14]. *top2-1* cells were inoculated at OD600 = 0.8 in BYTA medium for 20 hours at room temperature. For experiments that included *top2-1* mutants, SPO cultures for all strains were washed twice with water and resuspended into SPO medium at OD600 = 1.9 at room temperature and shifted to 34°C after 1 hour. For the Brn1-FRB anchor away experiment, rapamycin was added to a final concentration of 1μM at the time of meiotic induction (0h).

Chromosome spreads and immunofluorescence

Meiotic nuclear spreads were performed as described [45]. Red1 was detected using anti-Red1 rabbit serum (Lot#16441; kind gift of N. Hollingsworth) at 1:100 and Alexa Fluor 488 anti-rabbit antibody at 1:100. Microscopy and image processing were carried out using a Deltavision Elite imaging system (Applied Precision) adapted to an Olympus IX17 microscope and analyzed using softWoRx 5.0 software.

Chromatin immunoprecipitation

At the indicated time points (0 or 3h), 25 ml of meiotic culture was harvested and fixed for 30 min in 1% formaldehyde. Formaldehyde was quenched by addition of 125 mM glycine and samples processed as described [46]. Samples were immunoprecipitated with 2 μL of either anti-H3 (Abcam ab1791), anti-Hop1 (kind gift of N. Hollingsworth) or anti-Red1 (kind gift of N. Hollingsworth, #16440) per IP. Library preparation was completed as described [7]. Library quality

was confirmed by Qubit HS assay kit and either Agilent 2100 Bioanalyzer or 2200 TapeStation. 50bp or 51bp single-end sequencing was accomplished on an Illumina HiSeq 2500 or NextSeq 500 instrument. Read length and sequencing instrument did not introduce any obvious biases to the results.

Mononucleosomal DNA preparation

At the 0- or 3-hr time point, 50 ml of meiotic culture was harvested and fixed for 30 min in 1% formaldehyde. The formaldehyde was quenched by addition of 125 mM glycine and samples processed as described [25]. Library preparation and sequencing were done as outlined under the chromatin immunoprecipitation section above.

Processing of Illumina sequence data

Sequencing reads were mapped to the SK1 genome [47] using Bowtie. Sequencing reads of 100 bp were clipped to 51 bp. Only perfect matches across all 51 bp were considered during mapping. Multiple alignments were not taken into account, which means each read only mapped to one location in the genome. Reads were extended towards 3' ends to a final length of 200 bp and probabilistically determined PCR duplications were removed in MACS-2.1.1 (https://github.com/taoliu/MACS) [48]. All pileups were SPMR-normalized (signal per million reads), and fold-enrichment of the ChIP data over the input data was calculated. Plots shown were made using two or more combined replicates. The 95% confidence intervals were calculated by bootstrap resampling from the data 1000 times with replacement.

Peak Calling

To identify Red1, Hop1, and Rec8 protein enriched regions (peaks) for **Figure 1E**, MACS-2.1.1 (https://github.com/taoliu/MACS) [48] was used for peak calling of the sequence data. The reads were processed identically to the description in the "Processing of Illumina sequence data," except

the --broad flag was used with the "callpeak" function to determine significant regions of enrichment that meet the default q-value cutoff.

Defining clusters and deserts

The Red1 ChIP-seq sequencing data in the *rec8*Δ mutant was partitioned into 5000 bp bins with signal scores equal to the average signal across the bin. Bins with scores greater than or equal to 1.75 times the standard deviation of the Red1 signal across the genome were classified as enriched regions. Enriched regions were joined with adjacent enriched regions to define "clusters". The remaining regions were defined as "deserts".

Logistic regression modeling

The genome was divided into 5000 bp bins, matching the bins used to define clusters. Each bin was classified as either a cluster or a desert and the coding density was calculated for each bin. The caret package (https://github.com/topepo/caret/) was used to create a training set of 80% of the data and a test set of the remaining 20% of the data, and to train a logistic regression model using the training data. The coding density was determined to be a significant feature ($P<0.0001$). This model was applied to the test data to predict the cluster status using the input coding density.

Data Availability

The datasets and computer code produced in this study are available in following databases:

- ChIP-seq data data: Gene Expression Omnibus GSE156040 'https://www.ncbi.nlm.nih.gov/geo/query/acc.cgi?acc=GSE156040'
- Computer scripts for processing Illumina reads: Github 'https://github.com/hochwagenlab/ChIPseq_functions/tree/master/ChIPseq_Pipeline_v3/'

Computer scripts for making figures: Github 'https://github.com/hochwagenlab/axis_clusters '

References

1. Borde, V., and de Massy, B. (2013). Programmed induction of DNA double strand breaks during meiosis: Setting up communication between DNA and the chromosome structure. Current Opinion in Genetics and Development *23*, 147–155.
2. Lam, I., and Keeney, S. (2015). Mechanism and regulation of meiotic recombination initiation. Cold Spring Harbor Perspectives in Biology *7*.
3. Székvölgyi, L., Ohta, K., and Nicolas, A. (2015). Initiation of meiotic homologous recombination: Flexibility, impact of histone modifications, and chromatin remodeling. Cold Spring Harbor Perspectives in Biology *7*, 1–18.
4. Zickler, D., and Kleckner, N. (2015). Recombination, pairing, and synapsis of homologs during meiosis. Cold Spring Harbor Perspectives in Biology *7*, 1–28.
5. Page, S.L., and Hawley, R.S. (2004). THE GENETICS AND MOLECULAR BIOLOGY OF THE SYNAPTONEMAL COMPLEX. Annual Review of Cell and Developmental Biology *20*, 525–558. Available at: www.annualreviews.org [Accessed October 1, 2019].
6. Panizza, S., Mendoza, M.A., Berlinger, M., Huang, L., Nicolas, A., Shirahige, K., and Klein, F. (2011). Spo11-accessory proteins link double-strand break sites to the chromosome axis in early meiotic recombination. Cell *146*, 372–383.
7. Sun, X., Huang, L., Markowitz, T.E., Blitzblau, H.G., Chen, D., Klein, F., and Hochwagen, A. (2015). Transcription dynamically patterns the meiotic chromosome-axis interface. eLife *4*, e07424. Available at: http://www.ncbi.nlm.nih.gov/pubmed/26258962.
8. Kugou, K., Fukuda, T., Yamada, S., Ito, M., Sasanuma, H., Mori, S., Katou, Y., Itoh, T., Matsumoto, K., Shibata, T., *et al.* (2009). Rec8 guides canonical Spo11 distribution along yeast meiotic chromosomes. Mol Biol Cell *20*, 3064–3076.
9. Klein, F., Mahr, P., Galova, M., Buonomo, S.B.C., Michaelis, C., Nairz, K., and Nasmyth, K. (1999). A central role for cohesins in sister chromatid cohesion, formation of axial elements, and recombination during yeast meiosis. Cell *98*, 91–103.
10. Schalbetter, S.A., Fudenberg, G., Baxter, J., Pollard, K.S., and Neale, M.J. (2019). Principles of meiotic chromosome assembly revealed in S. cerevisiae. Nature Communications *10*.
11. Vale-Silva, L.A., Markowitz, T.E., and Hochwagen, A. (2019). SNP-ChIP: A versatile and tag-free method to quantify changes in protein binding across the genome. BMC Genomics *20*, 54. Available at: http://www.ncbi.nlm.nih.gov/pubmed/30654749.
12. Lambing, C., Tock, A.J., Topp, S.D., Choi, K., Kuo, P.C., Zhao, X., Osman, K., Higgins, J.D., Franklin, F.C.H., and Henderson, I.R. (2020). Interacting Genomic Landscapes of REC8-Cohesin, Chromatin, and Meiotic Recombination in Arabidopsis. The Plant cell.
13. Markowitz, T.E., Heldrich, J., and Hochwagen, A. (2020). DNA break formation induces Scc2/cohesin-dependent recruitment of condensin to meiotic chromosomes. bioRxiv *11*, 23–29.
14. Falk, J.E., Chan, A.C. ho, Hoffmann, E., and Hochwagen, A. (2010). A Mec1- and PP4-Dependent checkpoint couples centromere pairing to meiotic recombination. Developmental Cell *19*, 599–611.
15. Heldrich, J., Sun, X., Vale-Silva, L.A., Markowitz, T.E., and Hochwagen, A. (2020). Topoisomerases Modulate the Timing of Meiotic DNA Breakage and Chromosome Morphogenesis in Saccharomyces cerevisiae. Genetics.

16. Haruki, H., Nishikawa, J., and Laemmli, U.K. (2008). The Anchor-Away Technique: Rapid, Conditional Establishment of Yeast Mutant Phenotypes. Molecular Cell *31*, 925–932. Available at: http://www.ncbi.nlm.nih.gov/pubmed/18922474.
17. Paul, M., Markowitz, T.E., Hochwagen, A., and Ercan, S. (2018). Condensin Depletion Causes Genome Decompaction Without Altering the Level of Global Gene Expression in Saccharomyces cerevisiae. Genetics *210*, 331–344. Available at: http://www.ncbi.nlm.nih.gov/pubmed/29970489.
18. DiNardo, S., Voelkel, K., and Sternglanz, R. (1984). DNA topoisomerase II mutant of Saccharomyces cerevisiae: Topoisomerase II is required for segregation of daughter molecules at the termination of DNA replication. Proceedings of the National Academy of Sciences of the United States of America *81*, 2616–2620. Available at: http://www.ncbi.nlm.nih.gov/pubmed/6326134.
19. Blitzblau, H.G., Bell, G.W., Rodriguez, J., Bell, S.P., and Hochwagen, A. (2007). Mapping of Meiotic Single-Stranded DNA Reveals Double-Strand-Break Hotspots near Centromeres and Telomeres. Current Biology *17*, 2003–2012. Available at: http://www.ncbi.nlm.nih.gov/pubmed/18060788.
20. Subramanian, V. v, Zhu, X., Markowitz, T.E., Vale-Silva, L.A., San-Segundo, P.A., Hollingsworth, N.M., Keeney, S., and Hochwagen, A. (2019). Persistent DNA-break potential near telomeres increases initiation of meiotic recombination on short chromosomes. Nature Communications *10*, 970. Available at: http://www.ncbi.nlm.nih.gov/pubmed/30814509.
21. Murakami, H., Lam, I., Huang, P.C., Song, J., van Overbeek, M., and Keeney, S. (2020). Multilayered mechanisms ensure that short chromosomes recombine in meiosis. Nature *582*, 124–128.
22. Brogaard, K., Xi, L., Wang, J.P., and Widom, J. (2012). A map of nucleosome positions in yeast at base-pair resolution. Nature *486*, 496–501.
23. Zhu, X., and Keeney, S. (2015). High-resolution global analysis of the influences of Bas1 and Ino4 transcription factors on meiotic DNA break distributions in saccharomyces cerevisiae. Genetics *201*, 525–542. Available at: http://www.ncbi.nlm.nih.gov/pubmed/26245832.
24. Hu, J., Donahue, G., Dorsey, J., Govin, J., Yuan, Z., Garcia, B.A., Shah, P.P., and Berger, S.L. (2015). H4K44 Acetylation Facilitates Chromatin Accessibility during Meiosis. Cell Reports *13*, 1772–80.
25. Pan, J., Sasaki, M., Kniewel, R., Murakami, H., Blitzblau, H.G., Tischfield, S.E., Zhu, X., Neale, M.J., Jasin, M., Socci, N.D., *et al.* (2011). A hierarchical combination of factors shapes the genome-wide topography of yeast meiotic recombination initiation. Cell *144*, 719–731.
26. Cucinotta, C.E., Hildreth, A.E., McShane, B.M., Shirra, M.K., and Arndt, K.M. (2019). The nucleosome acidic patch directly interacts with subunits of the Paf1 and FACT complexes and controls chromatin architecture in vivo. Nucleic acids research *47*, 8410–8423.
27. Gothwal, S.K., Patel, N.J., Colletti, M.M., Sasanuma, H., Shinohara, M., Hochwagen, A., and Shinohara, A. (2016). The double-strand break landscape of meiotic chromosomes is shaped by the Paf1 transcription elongation complex in Saccharomyces cerevisiae. Genetics *202*, 497–512. Available at: http://www.ncbi.nlm.nih.gov/pubmed/26627841.

28. Thacker, D., Mohibullah, N., Zhu, X., and Keeney, S. (2014). Homologue engagement controls meiotic DNA break number and distribution. Nature *510*, 241–246. Available at: http://www.ncbi.nlm.nih.gov/pubmed/24717437.
29. Chen, S.Y., Tsubouchi, T., Rockmill, B., Sandler, J.S., Richards, D.R., Vader, G., Hochwagen, A., Roeder, G.S., and Fung, J.C. (2008). Global Analysis of the Meiotic Crossover Landscape. Developmental Cell *15*, 401–415. Available at: http://www.ncbi.nlm.nih.gov/pubmed/18691940.
30. Zhang, L., Wang, S., Yin, S., Hong, S., Kim, K.P., and Kleckner, N. (2014). Topoisomerase II mediates meiotic crossover interference. Nature *511*, 551–556. Available at: http://www.ncbi.nlm.nih.gov/pubmed/25043020.
31. Serrentino, M.E., Chaplais, E., Sommermeyer, V., and Borde, V. (2013). Differential Association of the Conserved SUMO Ligase Zip3 with Meiotic Double-Strand Break Sites Reveals Regional Variations in the Outcome of Meiotic Recombination. PLoS Genetics *9*, e1003416. Available at: https://dx.plos.org/10.1371/journal.pgen.1003416 [Accessed June 1, 2020].
32. Joshi, N., Barot, A., Jamison, C., and Börner, G.V. (2009). Pch2 links chromosome axis remodeling at future crossover sites and crossover distribution during yeast meiosis. PLoS Genetics *5*, 1000557. Available at: www.plosgenetics.org [Accessed October 15, 2019].
33. Börner, G.V., Barot, A., and Kleckner, N. (2008). Yeast Pch2 promotes domainal axis organization, timely recombination progression, and arrest of defective recombinosomes during meiosis. Proceedings of the National Academy of Sciences of the United States of America *105*, 3327–3332. Available at: http://www.ncbi.nlm.nih.gov/pubmed/18305165.
34. Kim, K.P., Weiner, B.M., Zhang, L., Jordan, A., Dekker, J., and Kleckner, N. (2010). Sister cohesion and structural axis components mediate homolog bias of meiotic recombination. Cell *143*, 924–937.
35. Yatskevich, S., Rhodes, J., and Nasmyth, K. (2019). Organization of Chromosomal DNA by SMC Complexes. Annu Rev Genet *53*, 445–482. Available at: http://www.ncbi.nlm.nih.gov/pubmed/31577909.
36. Uhlmann, F. (2016). SMC complexes: from DNA to chromosomes. Nat Rev Mol Cell Biol *17*, 399–412. Available at: http://www.ncbi.nlm.nih.gov/pubmed/27075410.
37. Wang, J.C. (2002). Cellular roles of DNA topoisomerases: A molecular perspective. Nature Reviews Molecular Cell Biology *3*, 430–440. Available at: http://www.ncbi.nlm.nih.gov/pubmed/12042765.
38. Pommier, Y., Sun, Y., Huang, S.Y.N., and Nitiss, J.L. (2016). Roles of eukaryotic topoisomerases in transcription, replication and genomic stability. Nature Reviews Molecular Cell Biology *17*, 703–721.
39. Primig, M., Williams, R.M., Winzeler, E.A., Tevzadze, G.G., Conway, A.R., Hwang, S.Y., Davis, R.W., and Esposito, R.E. (2000). The core meiotic transcriptome in budding yeasts. Nature Genetics *26*, 415–423.
40. Chu, S., DeRisi, J., Eisen, M., Mulholland, J., Botstein, D., Brown, P.O., and Herskowitz, I. (1998). The transcriptional program of sporulation in budding yeast. Science *282*, 699–705.
41. Kironmai, K.M., Muniyappa, K., Friedman, D.B., Hollingsworth, N.M., and Byers, B. (1998). DNA-Binding Activities of Hop1 Protein, a Synaptonemal Complex Component from Saccharomyces cerevisiae. Molecular and Cellular Biology *18*, 1424–1435.

42. Kshirsagar, R., Khan, K., Joshi, M. v., Hosur, R. v., and Muniyappa, K. (2017). Probing the Potential Role of Non-B DNA Structures at Yeast Meiosis-Specific DNA Double-Strand Breaks. Biophysical Journal *112*, 2056–2074.
43. Agarwal, S., and Roeder, G.S. (2000). Zip3 provides a link between recombination enzymes and synaptonemal complex proteins. Cell *102*, 245–255.
44. Subramanian, V. v., MacQueen, A.J., Vader, G., Shinohara, M., Sanchez, A., Borde, V., Shinohara, A., and Hochwagen, A. (2016). Chromosome Synapsis Alleviates Mek1-Dependent Suppression of Meiotic DNA Repair. PLoS Biology *14*, e1002369. Available at: http://www.ncbi.nlm.nih.gov/pubmed/26870961 [Accessed September 26, 2019].
45. Subramanian, V. v, MacQueen, A.J., Vader, G., Shinohara, M., Sanchez, A., Borde, V., Shinohara, A., and Hochwagen, A. (2016). Chromosome Synapsis Alleviates Mek1-Dependent Suppression of Meiotic DNA Repair. PLoS Biology *14*, e1002369. Available at: http://www.ncbi.nlm.nih.gov/pubmed/26870961.
46. Blitzblau, H.G., and Hochwagen, A. (2013). ATR/Mec1 prevents lethal meiotic recombination initiation on partially replicated chromosomes in budding yeast. eLife *2*, e00844. Available at: http://www.ncbi.nlm.nih.gov/pubmed/24137535.
47. Yue, J.X., Li, J., Aigrain, L., Hallin, J., Persson, K., Oliver, K., Bergström, A., Coupland, P., Warringer, J., Lagomarsino, M.C., *et al.* (2017). Contrasting evolutionary genome dynamics between domesticated and wild yeasts. Nature Genetics *49*, 913–924. Available at: http://www.ncbi.nlm.nih.gov/pubmed/28416820.
48. Zhang, Y., Liu, T., Meyer, C.A., Eeckhoute, J., Johnson, D.S., Bernstein, B.E., Nussbaum, C., Myers, R.M., Brown, M., Li, W., *et al.* (2008). Model-based analysis of ChIP-Seq (MACS). Genome Biology *9*, R137. Available at: http://www.ncbi.nlm.nih.gov/pubmed/18798982.